

# 光学学报

## 基于 AOTF 成像光谱仪主动变焦前置光学系统设计

常凌颖<sup>1\*</sup>, 王馨幼<sup>1</sup>, 邱跃洪<sup>2</sup>, 王冠儒<sup>1</sup>, 石浩楠<sup>1</sup>, 梁驰<sup>1</sup>, 陈奎<sup>1</sup>

<sup>1</sup> 西安邮电大学电子工程学院, 陕西 西安 710121;

<sup>2</sup> 中国科学院西安光学精密机械研究所, 西安 710119

**摘要** 声光可调协滤波器(AOTF)成像光谱仪可同时获取探测目标的空间图像和光谱信息, 具有体积小、质量轻、中心波长挑选灵活等优势。提出一种基于AOTF成像光谱仪组合变焦光学系统设计方案并完成了主动变焦前置光学系统仿真设计。该方案由主反式变焦前置系统和具有任意放大倍数的投影系统组成, 可实现大变焦范围主动变焦成像。前置光学系统的初始结构由主反式变焦系统设计理论确定, 利用同轴系统的离轴解和参数优化完成离轴三反远心结构的设计和系统像差校正, 构建逐步逼近优化法实现主动连续变焦。在Code V中的仿真结果表明: 前置变焦系统工作波段为0.5~1.7 μm, 变焦范围为260~520 mm, 短焦处调制传递函数大于0.68@34 lp/mm, 长焦处大于0.45@34 lp/mm, 全场的均方根半径小于0.345 μm, 成像质量良好。

**关键词** 声光可调协滤波器成像光谱仪; 光学设计; 组合主动变焦; 离轴三反; 像方远心

中图分类号 O439

文献标志码 A

DOI: 10.3788/AOS230664

### 1 引言

声光可调协滤波器(AOTF)成像光谱仪是一种非常高效的定量探测仪器, 可以获得探测目标的连续单色光谱图像, 提供探测目标的空间和光谱特征细节<sup>[1]</sup>。AOTF成像光谱仪是一款波段电子可调凝视光谱仪, 具有体积小、质量轻、中心波长挑选灵活、光谱采样步长可控、波长扫描快速, 以及环境适应性优秀等特点<sup>[2-3]</sup>, 被广泛应用于深空探测、测绘遥感、目标识别、环境监测与评估、临床影像诊断、过程监控等任务中<sup>[4-5]</sup>。

变焦系统具有连续可变的焦距, 可以有效地扩展AOTF成像光谱仪的成像功能, 可对目标物体进行连续探测、跟踪、识别和瞄准<sup>[6]</sup>。2013年, 崔成君<sup>[7]</sup>提出基于AOTF的超光谱变焦光学系统设计, 系统变焦范围为30~300 mm。2014年, 赵昭等<sup>[8]</sup>提出基于AOTF的光谱相机前置变焦光学系统设计, 变焦范围为15~300 mm。传统的机械变焦由运动光学元件实现<sup>[9]</sup>, 对于这种形式, 组元焦距固定不变, 但机械运动复杂, 变焦速率低, 响应速度慢。与传统变焦方式不同, 主动变焦不仅能够做到实时响应而且能提供较大范围的曲率变化, 是一种新型的快速成像方式。

主动变焦光学系统无运动部件, 通过控制主动光学元件的曲率、折射率等的变化实现系统光焦度的改变<sup>[10]</sup>。主动光学元件主要包括变形反射镜、液体透镜、

空间光调制器等, 其中, 变曲率反射镜(VCM)是变形反射镜的衍生, 又可称为变焦镜, 是反射式无运动变焦成像的关键器件。近年来, 随着国内外包括美国Sandia国家实验室、德国Dresden大学、北京理工大学以及中国科学院西安光学精密机械研究所等机构对无运动部件变焦技术研究的推进, 利用变曲率反射镜实现主动变焦技术已日趋成熟, 且其性能也逐渐提升<sup>[11-12]</sup>。

本文根据所研究AOTF成像光谱仪的工作原理、特性及技术指标, 设计了适用于AOTF成像光谱仪的前置主反式连续变焦光学系统, 该系统使用VCM实现变焦功能。

### 2 AOTF 成像光谱仪变焦光学系统设计方案

#### 2.1 AOTF 成像光谱仪工作原理

AOTF是一种基于声光效应, 由换能器、声光晶体( $\text{TeO}_2$ )、声吸收体等3部分组成的电子可调滤波器, 具有共线和非共线两种工作模式, 通常在反常布拉格衍射的非共线模式下工作, 工作原理如图1所示。换能器能够将所加载的电信号转换为同频率的超声波, 在声光体中超声波与入射光波产生非线性效应, 当超声波矢量与入射光矢量满足布拉格衍射条件时, 入射光将发生布拉格衍射, 衍射光以一定角度从晶体中透

收稿日期: 2023-03-13; 修回日期: 2023-04-03; 录用日期: 2023-04-26; 网络首发日期: 2023-05-08

基金项目: 国家自然科学基金(61475190)

通信作者: \*sophia\_chang@126.com

射出来,而未发生衍射的复色光(零级光)则沿原传播方向直接透射过晶体。两束衍射光为正交偏振的单色

光,一束为e光,一束为o光,分别位于零级光两侧,衍射光束与零级光束分离角随驱动频率变化<sup>[13]</sup>。

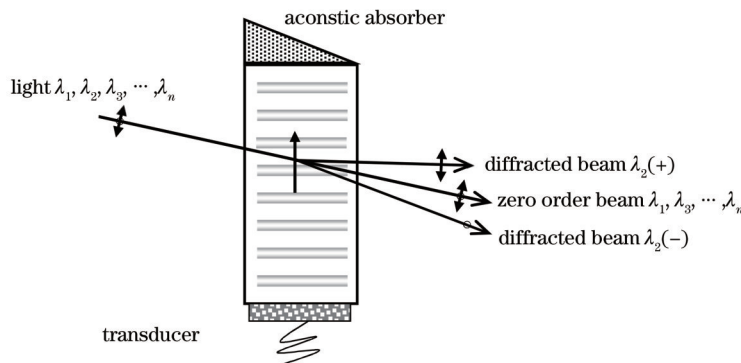


图 1 AOTF 工作原理  
Fig. 1 Principle of AOTF

AOTF 成像光谱仪由前置系统、AOTF、射频(RF)驱动器、投影系统、电子系统、中央处理器(CPU)组成,如图 2 所示。入射光通过前置系统到达 AOTF,在晶体中产生声光相互作用,再由电脑编程改变 RF

驱动信号选择通过 AOTF 的光波,最后,单色衍射光通过投影系统聚焦在探测器 CCD 上。电子系统给 CCD 和射频信号供电,并将输出的电信号转化为数字信号传送至计算机上。

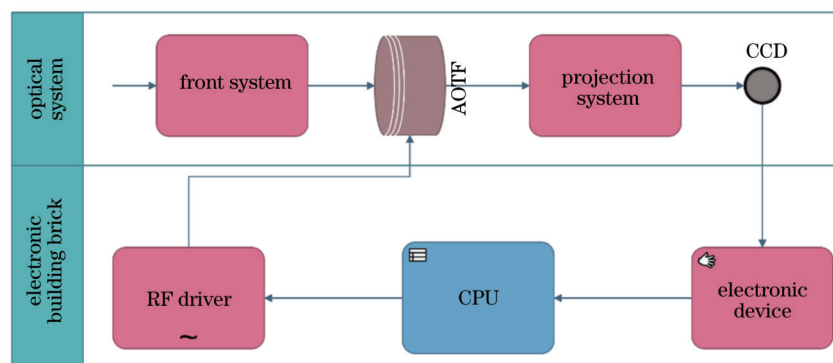


图 2 AOTF 成像光谱仪结构  
Fig. 2 The structure of AOTF imaging spectrometer

## 2.2 光学系统设计方案

在光学系统设计时,将晶体等效为平板以计算光学系统参数,但由于声光可调谐滤光器中采用的声光晶体工作原理的特殊性,需对光学结构和布局综合考虑。为提高 AOTF 成像光谱仪对不同距离的目标检测的成像性能,提出基于共焦结构的组合变焦设计方

案,AOTF 作为系统视场光阑,前置系统将无限远的目标成像到 AOTF 上,再由投影系统二次成像到 CCD 上,如图 3 所示,

该方案中,前置系统为反射式主动变焦光学系统,使用变曲率反射镜实现连续变焦,后可接任意放大倍数( $N$ )的投影系统,放大比由 CCD 靶面面积决定,有

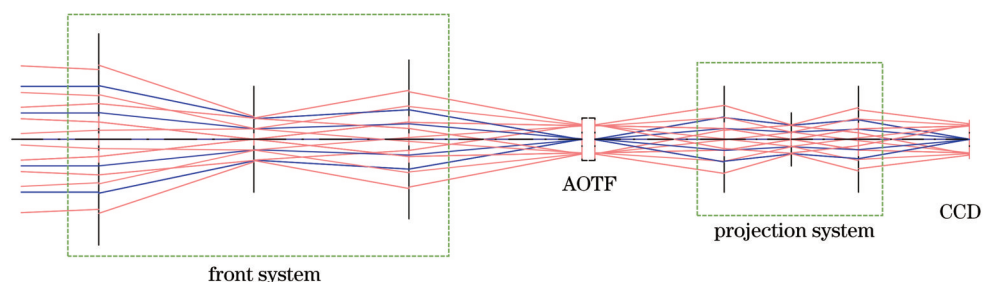


图 3 AOTF 成像光谱仪光学系统结构  
Fig. 3 Optical system structure of AOTF imaging spectrometer

效扩展变焦光学系统的变焦范围,实现具有大变焦范围的无运动部件主动变焦光学系统。前置变焦系统选用离轴三反光学结构(TMA),其具备宽光谱、大视场、高成像分辨率、易控制杂散光等特性,与AOTF成像光谱仪所需光学系统设计性能具有较高适配度。TMA可通过光阑离轴或视场离轴实现无中心遮拦,这有利于提高系统的光通量和点扩散函数质量<sup>[14-15]</sup>。

表1 AOTF和CCD器件的参数  
Table 1 Parameters of AOTF and CCD devices

CCD	Wavelength / μm	Resolution ratio	Pixel size / (μm × μm)
	0.4-1.7	640×512	15×15
AOTF	Work spectrum / μm	Crystal size / mm	Angle of incidence / (°)
	0.5-1.7	25	≤6

AOTF晶体在系统中为视场光阑,由于制作工艺的限制AOTF晶体尺寸不能做得足够大,通常可接收的光束角通常不大于6°,同时,受光线入射角度的影响,衍射效率、衍射带宽在3°以内时基本上没有变化,当入射角再增加1°时,则衍射带宽将增加50%,为保障衍射效率,入射角不得大于晶体可接收的光束角。此外,由于衍射光束与零级光束分离角随驱动频率变化,即使在AOTF设计时,加入消色散光楔,其衍射光束依然会随波长改变而产生会聚在焦面位置上的偏移,故在系统设计时预留空余接收靶面,即需相应地增加光学系统视场范围。综合以上维度的参数限定,光学系统的设计参数如表2所示。

### 3 光学系统设计与优化

#### 3.1 主反式变焦光学系统设计理论

计算主动变焦离轴三反光学系统的结构参数时,为

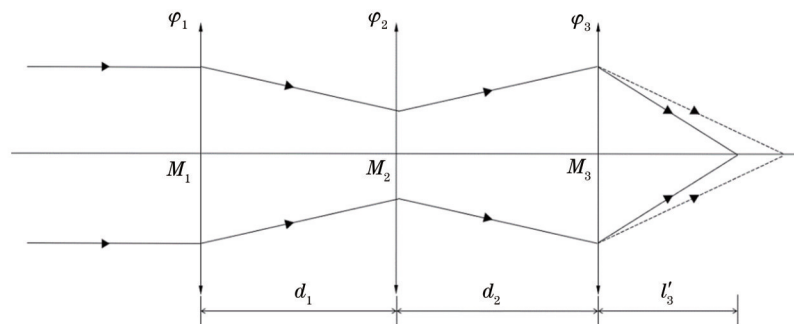


图4 三反射式变焦光学系统简化模型  
Fig. 4 Simplified model of TMA zoom system

$$\begin{cases} M_1 = \begin{pmatrix} 1 & 0 \\ -\varphi_1 & 1 \end{pmatrix} \\ M_2 = \begin{pmatrix} 1 & 0 \\ -\varphi_2 & 1 \end{pmatrix} \\ M_3 = \begin{pmatrix} 1 & 0 \\ -\varphi_3 & 1 \end{pmatrix} \end{cases} \quad (1)$$

根据选定的AOTF和CCD器件确定光学系统设计指标,具体参数如表1所示。考虑AOTF晶体尺寸和CCD靶面大小,假定投影系统的缩放比β为1,前置系统的像高由CCD器件靶面参数决定,为12.3 mm。为兼顾变焦系统的空间分辨率和发现识别目标的能力,设计变焦范围不小于100 mm,变倍比不小于2×,同时满足空间分辨率全焦范围内优于0.5 m@5 km。

表2 AOTF成像光谱仪光学系统设计参数

Table 2 Optical system design parameters of AOTF imaging spectrometer

Parameter	Value
Spectral band / μm	0.5-1.7
Focal length range / mm	260-520
Zoom range	2×
F number	6.5-13
FOV / (°)	2.7-1.3

数学上描述方便,忽略离轴和折叠,如图4所示。 $M_1$ 、 $M_2$ 、 $M_3$ 分别为主镜、次镜和三镜,各镜间间距为 $d_1$ 、 $d_2$ , $\varphi_1$ 、 $\varphi_2$ 、 $\varphi_3$ 分别代表3个反射镜的光焦度,图中正负透镜仅为示意,不代表实际光焦度的正负, $l'_3$ 代表系统的后截距。

根据矩阵光学理论,3个反射镜的光学变换矩阵可表示为

两镜之间的光学过渡矩阵可表示为

$$\begin{cases} T_1 = \begin{pmatrix} 1 & d_1 \\ 0 & 1 \end{pmatrix} \\ T_2 = \begin{pmatrix} 1 & d_2 \\ 0 & 1 \end{pmatrix} \end{cases} \quad (2)$$

因此整个系统的光学变换矩阵可表示为

$$\mathbf{M} = \begin{pmatrix} A & B \\ C & D \end{pmatrix} = \mathbf{M}_3 \mathbf{T}_2 \mathbf{M}_2 \mathbf{T}_1 \mathbf{M}_1 = \begin{pmatrix} 1 & 0 \\ -\varphi_{3i} & 1 \end{pmatrix} \begin{pmatrix} 1 & d_2 \\ 0 & 1 \end{pmatrix} \begin{pmatrix} 1 & 0 \\ -\varphi_{2i} & -1 \end{pmatrix} \begin{pmatrix} 1 & d_1 \\ 0 & 1 \end{pmatrix} \begin{pmatrix} 1 & 0 \\ -\varphi_1 & 1 \end{pmatrix}, \quad (3)$$

$$A = 1 - d_2 \varphi_{2i} - [(1 - d_2 \varphi_{2i})d_1 + d_2] \varphi_1, \quad (4)$$

$$B = (1 - d_2 \varphi_{2i})d_1 + d_2, \quad (5)$$

$$C = -\varphi_{3i} - (-\varphi_{3i}d_2 + 1)\varphi_{2i} - \{[-\varphi_{3i} - (-\varphi_{3i}d_2 + 1)\varphi_{2i}]d_1 - \varphi_{3i}d_2 + 1\} \varphi_1, \quad (6)$$

$$D = [-\varphi_{3i} - (-\varphi_{3i}d_2 + 1)\varphi_{2i}]d_1 - \varphi_{3i}d_2 + 1. \quad (7)$$

由式(3)可知,系统总光焦度和后截距为

$$F' = -1 / -\varphi_3 - (-\varphi_3d_2 + 1)\varphi_2 - \{[-\varphi_3 - (\varphi_3d_2 + 1)\varphi_2]d_1 - \varphi_3d_2 + 1\} \varphi_1, \quad (8)$$

$$l'_3 = F' \{1 - \varphi_2d_2 - [(1 - \varphi_2d_2)d_1 + d_2]\varphi_2\}. \quad (9)$$

主动变焦系统需要固定各反射镜间的距离,即间隔 $d_1, d_2$ 以及后截距 $l'_3$ 均保持不变,仅改变各镜曲率半径,即改变各镜的光焦度 $\varphi_1, \varphi_2, \varphi_3$ 来达到变焦效果。根据式(8)和式(9)结合三阶像差理论,即可得到三反射主动变焦系统的初始结构<sup>[16]</sup>。在前置主反式变焦光学系统中,设计主镜和次镜为补偿组,三镜为变倍组,系统采用“+,-,+”的光焦度分配方式,即 $F'_{(1-2i)} < 0, \varphi_3 > 0$ ,为反摄远型结构。该结构形式的一个优势在于易于扩大系统的视场,为视场离轴系统提供了视场角的选择性,以更高的视场离轴量实现系统无遮拦,可以减少反射镜的偏移和偏心量。

### 3.2 光学系统设计优化

#### 3.2.1 逐步逼近法

为提升优化的速率和精度,提出逐步逼近法对连续变焦光学系统进行优化。首先以 $f' = 260 \text{ mm}$ 、 $f' = 390 \text{ mm}$ 、 $f' = 520 \text{ mm}$ 处初始结构为起点,以 $1 \text{ mm}$ 为步长,以 $10$ 步为单位,采用断点法优化至新节点,即取三面镜面曲率半径为变焦变量( $R_1, R_2, R_3$ ),以某一焦距 $f' = x$ 为起点、 $f' = x + 1$ 为优化目标,在起点焦距系统结构的基础上,直接优化,获得焦距 $f' = x + 1$ 的系统结构,再以 $f' = x + 1$ 焦距为起点、 $f' = x + 2$ 为优化目标,逐步优化。得到新节点后,再共同优化新增节点与初始起点结构,即取三面镜面曲率半径为变焦变量,其余变量为普通变量(不随焦距变化而变化),包括镜面间距( $d_1, d_2, d_3$ )和镜面面型参数。循环往复至起点和所有节点处结构均完成同时优化,最后以断点法重新优化节点之间所有焦点位的结构,完成所有焦距处的光学结构设计。

#### 3.2.2 同轴系统离轴解

采用同轴系统离轴化,基于光学系统设计理论求解同轴系统结构参数,通过添加视场离轴,并且取适当的偏心和倾斜量消除系统中的光线遮拦,得到离轴三反变焦系统的初始结构。离轴化为各元件的空间布局提供了更多的可能性,但系统的结构类型和面型的选取都会影响系统最终的成像性能。

离轴系统在优化时会出现同轴化的趋势,通过约束各元件的偏心和倾斜量以及系统离轴量来确保离轴系统结构的稳定。在Code V软件设计时通过函数@JMRCC实现:入射光上边缘光线低于次镜下边缘点;出射光下边缘光线高于次镜上边缘点;主、三镜无重叠。在上述约束基础上进一步优化系统像质,以合理的布局做到光线无遮拦和高成像质量的兼顾。

#### 3.2.3 光学远心

对于共焦结构,入射光线经由前置系统以非平行光进入AOTF,当入射角和声波波长固定时,衍射角随波长变化,产生AOTF衍射像差,为此引入远心结构,可有效降低因AOTF中衍射特性产生的额外像差。同时,设计前置系统为像方远心光学结构,与AOTF和投影系统连接时,主光线的位置不随目标物体位置而变化,不影响物体高度测量,可有效消除视差,为后续衔接投影系统和系统的加工增加便利。

#### 3.2.4 像差平衡优化

更改光线入射到镜子的角度和镜间距,可以有效消除离轴系统的线性像散。添加非球面,可以更好地平衡和校正系统的轴外像差。目前,最常用的旋转对称非球面为基于偶次幂级数多项式的非球面<sup>[17-18]</sup>,具有较高设计自由度,并且更有利于校正像差以及提高光学系统的像质。系统较大的离轴量带来不可忽视的畸变问题,且畸变对光阑位置非常敏感,系统尽量趋于对称结构,即主次镜曲率半径趋于一致,主镜到次镜和次镜到三镜距离趋于一致,可以很好地控制系统畸变问题。

## 4 设计结果和像质评价

AOTF成像光谱仪前置变焦系统是基于变曲率反射镜的主动变焦光学系统,采用气压驱动结合变厚度结构使得反射镜的曲率半径改变以实现变焦功能,变焦过程中非球面系数不发生变化,仅改变反射镜的曲率半径。反射镜变焦过程中产生的最大中心形变量分别为 $44.2 \mu\text{m}$ 、 $73 \mu\text{m}$ 、 $603 \mu\text{m}$ ,因变焦产生中心形变引起的镜间距的变化量分别为 $0.029\%$ (主次镜间)、 $0.048\%$ (次镜与三镜间),面形精度优于 $0.0556\lambda$ 。

光学系统采用像方远心离轴三反结构,主镜、次镜和三镜变曲率反射镜均采用8阶高次非球面,以满足对光学成像质量的要求,光阑位于次镜附近,具有较好的对称性,结构紧凑。表3是前置变焦系统结构参数,

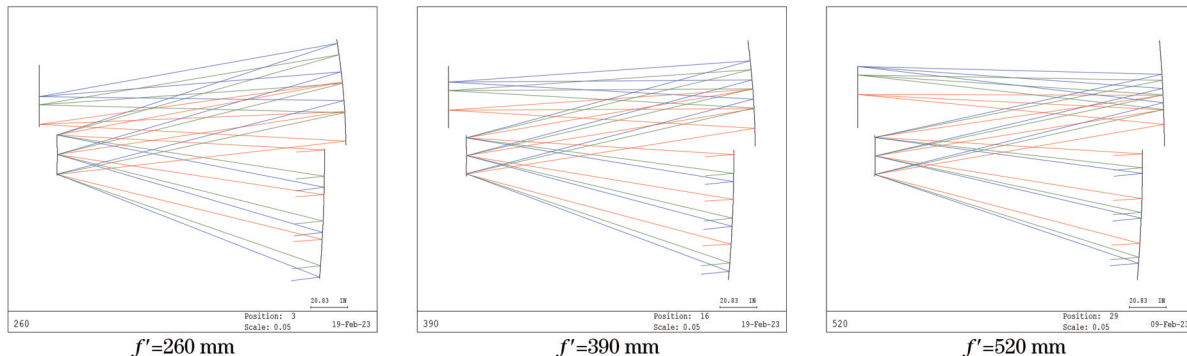


图5 前置系统光线追迹图

Fig. 5 Optical layouts of the zoom front system

表3 前置系统结构参数

Table 3 Parameters of the zoom front system

	Radius of curvature $R$ /mm			Diameter /mm
	Wide Angle	Mid-zoom	Tele-zoom	
Mirror 1	-540.4	-512.1	-516.5	55
Mirror 2(stop)	-173.9	-189.5	-247.3	9
Mirror 3	-255.0	-299.8	-470.8	52
	Distance /mm			
Mirror 1-mirror 2		-150.8		
Mirror 2-mirror 3		162.9		
Mirror 3-image		-173.1		

图6为三面变曲率反射镜的中心形变量 $\Delta$ 与焦距 $f$ 变化关系图, $R_1$ 、 $R_2$ 、 $R_3$ 分别为主镜、次镜和三镜。 $f$ 变化范围为260~520 mm, $R_1$ 、 $R_2$ 、 $R_3$ 的中心形变量分别为44.2 μm、73 μm、603 μm,具备切实可行的制造能力。系统变焦过程中, $R_1$ 、 $R_2$ 、 $R_3$ 和 $f$ 均连续变化,变焦曲线平滑,无跳跃值,可以减轻反射镜变形过程的负担,提升反应速度。图7为前置系统短焦、中焦和长焦3个变焦位置处的调制传递函数(MTF)曲线。0.5~1.7 μm工作波段在空间频率34 lp/mm处,光学系统在短焦时,MTF大于0.68,中焦时,MTF大于0.62,长焦时,MTF大于0.45,接近衍射极限。图8为各个变焦位置处的点列图,全视场范围内短焦处弥散斑小于0.193 μm,中焦处弥散斑小于0.196 μm,长焦处弥散斑小于0.345 μm。

## 5 结 论

提出一种基于AOTF成像光谱仪的组合式变焦光学系统设计方案,采用前置变焦系统与不同倍率的投影系统的组合来获取更大的变焦范围,并提供一个适用于AOTF成像光谱仪的前置变焦光学系统

图5为前置变焦系统光线追迹图,连续变焦范围为260~520 mm,变倍比为2×,视场角为2.7°~1.3°,入瞳直径为40 mm,F数为6.5~13,像面平稳,系统体积为117 mm×107 mm×55 mm。

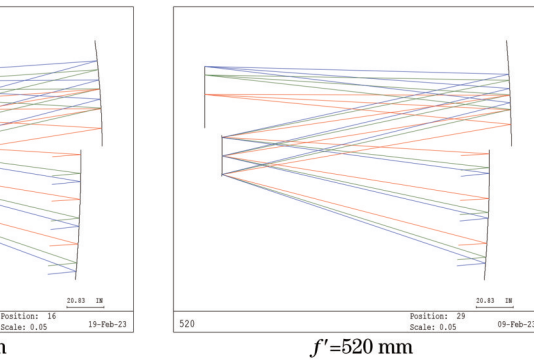
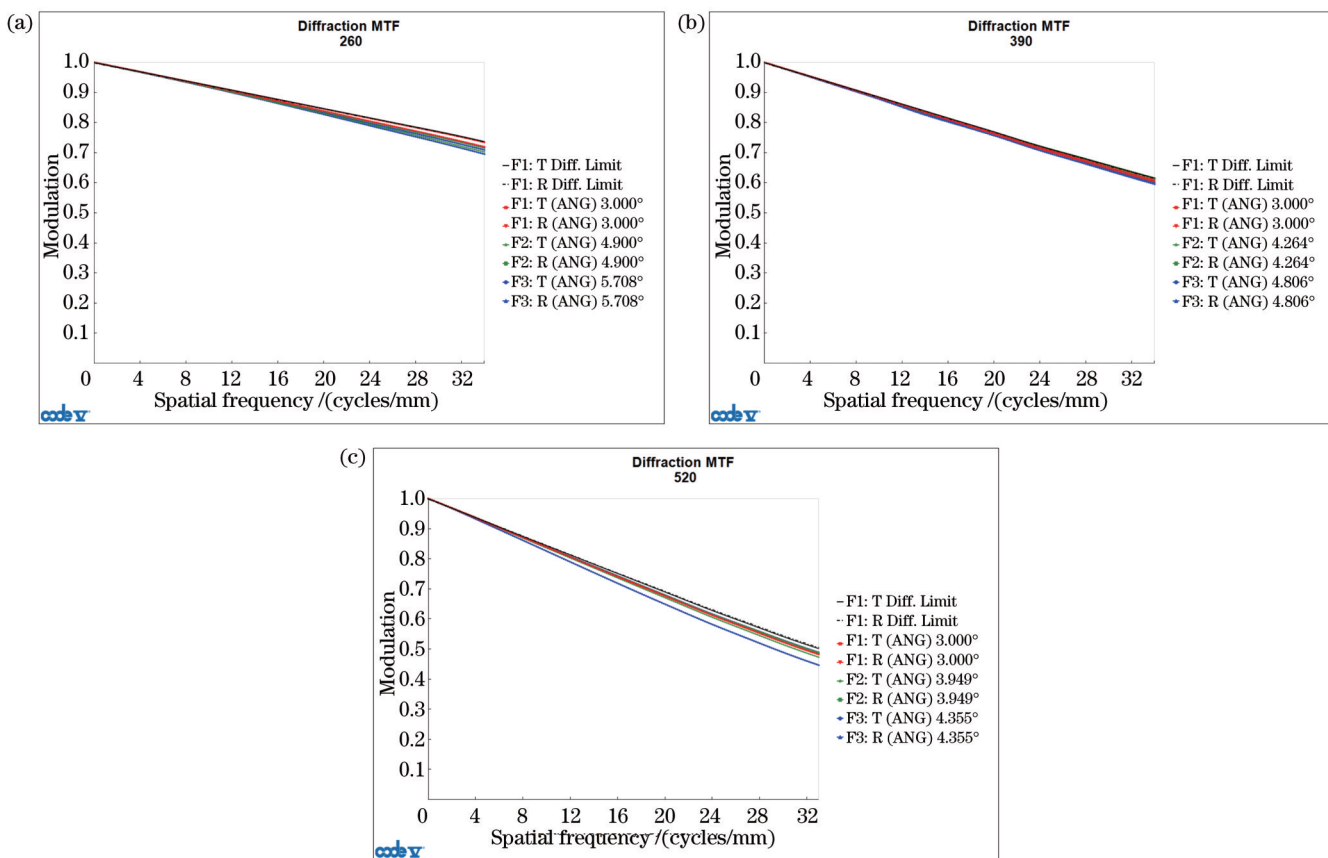
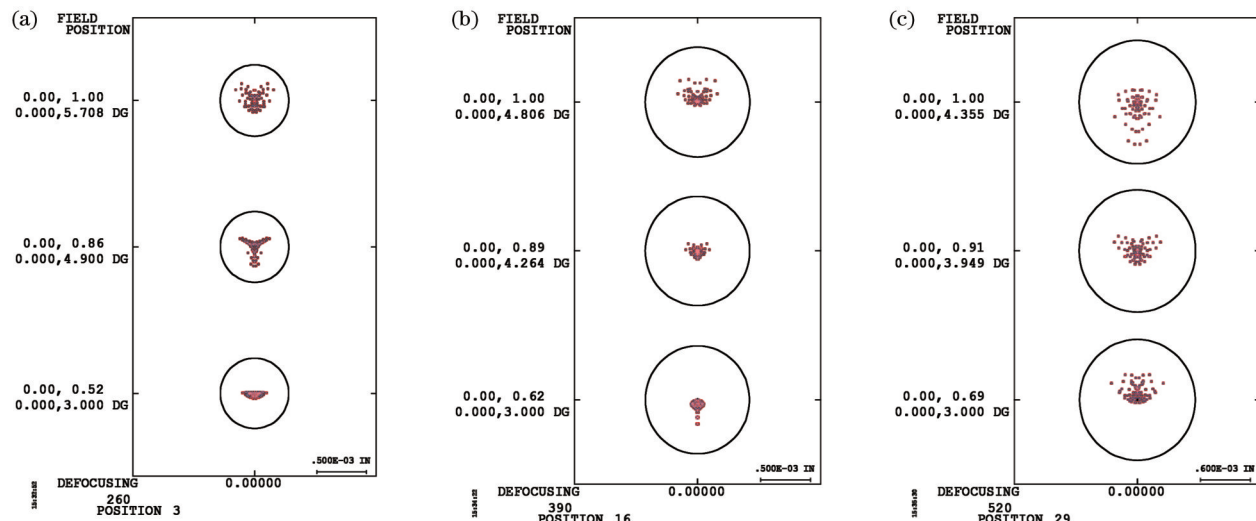


图6 镜面中心形变与焦距变化关系图

fig. 6 Relation between focal length and center shape variable

设计实例:采用同轴系统的离轴解和逐步逼近优化法实现离轴三反式前置连续变焦光学系统。此外,前置变焦系统为准像方远心光学结构,可为后续衔接投影系统的工作提供便利。光学系统工作波长为0.5~1.7 μm,变焦范围为260~520 mm,具有平滑的变焦曲线和稳定的像面,变曲率反射镜设计参数具有可实现性。成像质量优良:短焦时,MTF大于0.68@34 lp/mm;中焦时,MTF大于0.62@34 lp/mm;长焦

图 7 MTF。(a) $f'=260$  mm; (b) $f'=390$  mm; (c) $f'=520$  mmFig. 7 MTF. (a) $f'=260$  mm; (b) $f'=390$  mm; (c) $f'=520$  mm图 8 点列图。(a) $f'=260$  mm; (b) $f'=390$  mm; (c) $f'=520$  mmFig. 8 Spot diagrams. (a) $f'=260$  mm; (b) $f'=390$  mm; (c) $f'=520$  mm

时, MTF 大于 0.45@34 lp/mm。全场均方根半径小于 0.345  $\mu\text{m}$ 。系统结构紧凑、全电调谐、响应速度快、体积小、质量轻, 可灵活应用于多种探测场景中。

## 参 考 文 献

- [1] 于磊. 成像光谱仪的发展与应用[J]. 红外与激光工程, 2022, 51(1): 20210940.

- Yu L. Development and application of imaging spectrometer[J]. Infrared and Laser Engineering, 2022, 51(1): 20210940.  
[2] Xu R, He Z P, Zhang H, et al. Calibration of imaging spectrometer based on acousto-optic tunable filter (AOTF)[J]. Proceedings of SPIE, 2012, 8527: 85270S.  
[3] He Z P, Zhao H T, Li J N. Characteristics of staring imaging spectrometer and its application prospect in asteroid exploration [J]. Aerospace China, 2019, 20(3): 14-21.  
[4] Warren M A, Simis S G H, Martinez-Vicente V, et al.

- Assessment of atmospheric correction algorithms for the Sentinel-2A MultiSpectral Imager over coastal and inland waters[J]. *Remote Sensing of Environment*, 2019, 225: 267-289.
- [5] Xu Z F, Zhao H J, Jia G R, et al. Optical schemes of super-angular AOTF-based imagers and system response analysis[J]. *Optics Communications*, 2021, 498: 127204.
- [6] 石濮瑞. 无运动部件反射式变焦光学系统研究[D]. 北京: 北京理工大学, 2015.
- Shi P R. Research on reflective zoom optical system without moving parts[D]. Beijing: Beijing Institute of Technology, 2015.
- [7] 崔成君. 基于 AOTF 的超光谱变焦光学系统设计[D]. 长春: 长春理工大学, 2013.
- Cui C J. Optical design of hyperspectral zoom system base on AOTF[D]. Changchun: Changchun University of Science and Technology, 2013.
- [8] 赵昭, 安志勇, 高铎瑞, 等. AOTF 光谱相机前置变焦光学系统设计[J]. *应用光学*, 2014, 35(4): 580-585.
- Zhao Z, An Z Y, Gao D R, et al. Design of fore continuous zoom optical system of AOTF spectral camera[J]. *Journal of Applied Optics*, 2014, 35(4): 580-585.
- [9] 同阿奇, 崔雯, 董森. 大变倍比光学被动半无热化变焦系统设计[J]. *光学学报*, 2022, 42(4): 0422001.
- Yan A Q, Cui W, Dong S. Optical design of optical passive half-athermalization zoom lens with high zoom ratio[J]. *Acta Optica Sinica*, 2022, 42(4): 0422001.
- [10] 解晓蓬. 变曲率反射镜形变机理及优化设计研究[D]. 西安: 中国科学院西安光学精密机械研究所, 2020.
- Xie X P. Deformation mechanism and optimization design of variable curvature mirror[D]. Xi'an: Xi'an Institute of Optics and Fine Mechanics, Chinese Academy of Sciences, 2020.
- [11] 赵惠. 用于无运动部件变焦的变曲率反射镜技术研究[D]. 西安: 中国科学院西安光学精密机械研究所, 2020.
- Zhao H. Research on variable curvature mirror technology for zoom without moving parts[D]. Xi'an: Xi'an Institute of Optics and Fine Mechanics, Chinese Academy of Sciences, 2020.
- [12] 赵惠, 解晓蓬, 高立民, 等. 变厚变曲率反射镜及其在空间相机中的应用[J]. *光学学报*, 2022, 42(17): 1723002.
- Zhao H, Xie X P, Gao L M, et al. Variable thickness and curvature mirror and its application in space camera[J]. *Acta Optica Sinica*, 2022, 42(17): 1723002.
- [13] 常凌颖, 张强, 邱跃洪. 宽谱段一体化 AOTF 成像光谱仪光学系统设计[J]. *光学学报*, 2021, 41(7): 0722002.
- Chang L Y, Zhang Q, Qiu Y H. Design of optical system for broadband and integrated AOTF imaging spectrometer[J]. *Acta Optica Sinica*, 2021, 41(7): 0722002.
- [14] 罗敬, 王金鑫, 鞠国浩, 等. 主动随机送风条件下大口径离轴三反光学系统的计算机辅助装调[J]. *光学精密工程*, 2022, 30(7): 802-812.
- Luo J, Wang J X, Ju G H, et al. Computer-aided alignment for large-aperture off-axis three mirrors optical system with artificially random air flow[J]. *Optics and Precision Engineering*, 2022, 30(7): 802-812.
- [15] 杨增鹏, 李政言, 浦恩昌, 等. 基于离轴三反光学系统的高分辨率中阶梯光栅光谱仪[J]. *光学学报*, 2021, 41(22): 2212001.
- Yang Z P, Li Z Y, Pu E C, et al. High-resolution echelle grating spectrometer based on off-axis three-mirror reflective optical system[J]. *Acta Optica Sinica*, 2021, 41(22): 2212001.
- [16] 常军, 沈本兰, 王希, 等. 宽谱段、动态局部高分辨离轴主动反射变焦系统[J]. *光学精密工程*, 2016, 24(1): 7-13.
- Chang J, Shen B L, Wang X, et al. Off-axis reflective active zoom system with broad spectrum and dynamic local high-resolution[J]. *Optics and Precision Engineering*, 2016, 24(1): 7-13.
- [17] 张学军. 空间光学系统先进制造技术进展——从非球面到自由曲面[J]. *光学学报*, 2023, 43(8): 0822009.
- Zhang X J. Progress on space optics manufacturing: from aspheres to freeforms[J]. *Acta Optica Sinica*, 2023, 43(8): 0822009.
- [18] 刘锦琳, 余飞鸿. 旋转对称非球面表述及其特点分析[J]. *激光与光电子学进展*, 2021, 58(9): 0922001.
- Liu J L, Yu F H. Descriptions of rotationally symmetric aspheres and analysis of their characteristics[J]. *Laser & Optoelectronics Progress*, 2021, 58(9): 0922001.

## Optical Design of Active Zoom Front System for AOTF Imaging Spectrometer

Chang Lingying<sup>1\*</sup>, Wang Xinyou<sup>1</sup>, Qiu Yuehong<sup>2</sup>, Wang Guanru<sup>1</sup>, Shi Haonan<sup>1</sup>, Liang Chi<sup>1</sup>, Chen Kui<sup>1</sup>

<sup>1</sup>College of Electronic Engineering, Xi'an University of Posts and Telecommunications, Xi'an 710121, Shaanxi, China;

<sup>2</sup>Xi'an Institute of Optics and Precision Mechanics of CAS, Xi'an 710119, Shaanxi, China

### Abstract

**Objective** The acousto-optic tunable filter (AOTF) spectrometer can simultaneously acquire the spatial image and spectral information of the detection target, featuring small size, light weight, and flexible selection of central wavelength. The optical system is an essential part of the information obtained by the AOTF imaging spectrometer, and its design scheme and imaging quality can affect the instrument's performance. The zoom system has continuously variable focal lengths. A suitable zoom system can effectively expand the imaging function of the AOTF spectrometer and realize continuous detection, tracking, recognition, and collimation of the target object. The zoom optics of current AOTF spectrometers is mostly mechanical zoom. The mechanical zoom system can modify the focal length only by changing the distance between the components. In contrast, the active zoom system without moving parts can adjust the focus by controlling the changes in curvature and refractive index of the active optical elements. In this study, we propose a design scheme of a combined zoom optical system of AOTF imaging spectrometer, which consists of an active zoom front optical

system and a projection system with arbitrary magnification ( $N$ ) to achieve a wide range of zoom, and the simulation design of active zoom front system is completed.

**Methods** First, the structure and working principle of the AOTF imaging spectrometer are investigated to determine the optical system design scheme, and the design theory of the off-axis three-mirror active zoom optical system is studied in detail to determine the initial structure of the zoom front system. Then, the off-axis field of view (FOV), eccentricity, and tilt of the mirror are added to remove the central light obstruction, which provides more possibilities for the spatial layout of each component. It tends to be coaxial after optimization, and the mirror must be constrained in the tilt and processed by decentration by using the @JMRCC macro function. After that, a progressive approximation is used to implement the continuous zoom function of the front optical system. Starting from the calculation solution of the initial structure at the system's short focus, medium focus, and long focus, the optimization criteria of node addressing and synchronous optimization alternating cycles are used to optimize optical structures at all focal lengths within the zoom range. In addition, the front system is an image space telecentric optical structure, which can effectively reduce the extra aberration caused by the diffraction in AOTF, eliminate parallax, and increase the convenience for the subsequent connection of the projection system and the processing of the system. Last, the linear astigmatism of the TMA is eliminated effectively by debugging the parameters of the incident angle and mirror spacing, and the off-axis aberration of the system is balanced and corrected by adding aspheric surfaces, which are based on even power series polynomials with rotational symmetry, and the design of the system tends to be symmetrical as much as possible control the system distortion problem.

**Results and Discussions** The active zoom front system adopts Cook-TMA with no intermediate image plane based on a variable curvature mirror (VCM), which changes the radius of curvature of the mirror to achieve zoom function (Fig. 5). The maximum central deformations of the mirrors are  $44.2\text{ }\mu\text{m}$ ,  $73\text{ }\mu\text{m}$ , and  $603\text{ }\mu\text{m}$ , respectively. The variations of mirror spacing caused by the deformation of mirrors are 0.029% (between primary and secondary mirror) and 0.048% (between secondary and third mirror), and the accuracy of surface shape is better than  $0.0556\lambda$ . In the process of system zoom, the mirror curvature radius and focal length are continuously changed, and the zoom curve is smooth without jumping value (Fig. 6). Three mirrors use 8th high-order aspheric surfaces, and coefficients are unchanged during the zoom process. The system is the image-side telecentric structure, and the stop is located in the secondary mirror with a small size, light weight, and compact structure. The results of the design in Code V show that the modulation transfer function (MTF) of zoom front system is greater than  $0.68@34\text{ lp/mm}$  on short focal length,  $0.62@34\text{ lp/mm}$  on middle one, and  $0.45@34\text{ lp/mm}$  on long one with 260–520 mm zoom range and 0.5–1.5  $\mu\text{m}$  spectral region (Fig. 7), and root mean square (RMS) radius is less than  $0.193\text{ }\mu\text{m}$  at the short focus,  $0.196\text{ }\mu\text{m}$  at the middle focus, and  $0.345\text{ }\mu\text{m}$  at the long focus (Fig. 8).

**Conclusions** In the present study, a design scheme of a combined zoom optical system for an AOTF imaging spectrometer is presented, which uses a combination of the active front zoom system with different magnifications of the projection system to obtain a larger zoom range, and a design example of a front zoom optical system for AOTF imaging spectrometer is provided. It uses the off-axis method of the coaxial system and the progressive approximation method to realize the off-axis three-mirror active continuous zoom optical system. The system is an image-side telecentric structure, which can effectively increase the convenience for the subsequent connection of the projection system and the processing of the system. The optical system has a working band of 0.5–1.7  $\mu\text{m}$ , a zoom range of 260–520 mm, a smooth zoom curve, and a stable image plane with realizable parameters of the VCM. The simulation result shows that the MTF is greater than  $0.45@34\text{ lp/mm}$ , and the RMS radius is less than  $0.345\text{ }\mu\text{m}$  in the full field. The system has a compact structure, with the characteristic of full-electric tuning, fast response speed, small size, and light weight, which can be flexibly applied to a variety of detection scenarios.

**Key words** AOTF imaging spectrometer; optical design; combined active zoom; off-axis three-mirror; image-side telecentric system